

Stable cobalt nanoparticles passivated with oleic acid and triphenylphosphine

H T Yang¹, C M Shen¹, Y G Wang², Y K Su^{1,3}, T Z Yang¹ and H J Gao¹

¹ Nanoscale Physics and Devices Laboratory, Institute of Physics, Chinese Academy of Sciences, Beijing 100080, People's Republic of China

² Beijing Laboratory of Electron Microscopy, Institute of Physics, Chinese Academy of Sciences, Beijing 100083, People's Republic of China

³ Department of Chemistry, Lanzhou University, Lanzhou 730000, People's Republic of China

E-mail: hjgao@aphy.iphy.ac.cn

Received 29 May 2003, in final form 14 August 2003

Published 10 November 2003

Online at stacks.iop.org/Nano/15/70 (DOI: 10.1088/0957-4484/15/1/014)

Abstract

Monodisperse cobalt nanoparticles (NPs) are synthesized via a high-temperature thermal decomposition method in the presence of oleic acid and triphenylphosphine. The as-synthesized NPs are stable against further deep oxidation when they are kept in heptane (C₇H₁₆). Time-dependent x-ray photoelectron spectroscopy studies indicate that the oxidation of the as-synthesized cobalt NPs by air is slow and the valence change of cobalt from the Co NP sample kept in heptane under air is not observed for 120 days. The cobalt NPs have β -manganese type structure (also called ϵ -cobalt). Annealing the NPs at 500 °C under Ar (95%) + H₂ (5%) converts these particles from ϵ -Co to fcc-Co. Two-dimensional (2D) and three-dimensional (3D) self-assembled superlattices of passivated cobalt NPs are formed by slow evaporation of the carrier solvent.

1. Introduction

Research on monodisperse magnetic nanoparticles (NPs) has been an extremely active area due to the potential applications of these particles in information data storage [1–6]. In order to prepare monodisperse magnetic NPs and obtain the ordered 2D or 3D self-assembled superlattices, the NPs need to be coated with organic surfactants to prevent them from irreversible aggregation [7–9]. The triphenylphosphine (TPP) has been widely used in the synthesis of phosphine-stabilized gold or other metal NPs [10–14]. The phenyl group in TPP can provide greater steric hindrance than the straight-chained alkyl group, such as tributylphosphine and trioctylphosphine, to control the size of nonmagnetic metal NPs, and may efficiently stabilize the magnetic NPs as well. However, the synthesis of magnetic NPs using TPP as a stabilizer has not been reported so far [15].

In this paper, we report the synthesis of cobalt NPs by thermal decomposition of cobalt carbonyl in the presence of TPP and oleic acid (OA) [16, 17]. The TPP and OA are employed as a stabilizer to control particle growth, to stabilize

the particles, and to prevent particles from oxidation. The cobalt NPs are synthesized by injecting the organometallic precursor into the surfactant mixture of TPP and OA at 200 °C and keeping the growth temperature at 180 °C under an inert environment. X-ray photoelectron spectroscopy (XPS), x-ray diffraction (XRD) and infrared (IR) spectrum are employed to characterize the structure and surfactants of the cobalt NPs. After the size range of the cobalt NPs is further narrowed through size-selective precipitation, two-dimensional (2D) and three-dimensional (3D) superlattice structures are obtained by controlled solvent evaporation.

2. Experiments

Cobalt octacarbonyl [Co₂(CO)₈], TPP (C₁₈H₁₅P), OA (C₁₈H₃₄O₂), dichlorobenzene (C₆H₄Cl₂) and heptane (C₇H₁₆) are obtained from ACROS Chemicals. All the reagents are used as received without further purification. To synthesize 6–8 nm Co NPs, a three-neck-flask with 40 ml of dichlorobenzene is heated to ~220 °C under N₂ and stirred

for a certain time to eliminate dissolved ambient air, then OA of 2.0 mmol and TPP of 2.0 mmol are added. In a separate reaction vessel, 2.0 mmol of $\text{Co}_2(\text{CO})_8$ is combined with 5 ml of dry dichlorobenzene, warmed briefly to nearly 60°C under N_2 until it is fully dissolved, and finally rapidly injected into the flask. The solution turns black quickly and foams as $\text{Co}_2(\text{CO})_8$ decomposes, nucleating Co NPs and releasing gas. After the CO disappears, the black solution is refluxed at 185°C for 20 min under vigorous stirring. Then the black solution is cooled down to room temperature, and a black precipitate appears by adding ethanol to the dispersion. The black precipitate is collected by centrifugation and washed with ethanol several times to remove excessive surfactant. The black magnetic precipitate is in turn redispersed in heptane and precipitated partially by slow titration of ethanol. Centrifuging the suspension isolates a precipitate enriched in the large NPs (30 wt%) and leaves small NPs (70 wt%) in the supernatant. Additional ethanol is added to the supernatant to isolate a second fraction of small NPs. Cobalt NPs with, on average, 7 nm diameter are obtained by the gentle destabilization/redispersion procedure with a size distribution of $\sigma \sim 5\%$. When increasing the concentration of TPP and OA by a factor of 2, cobalt NPs with an average 5 nm diameter can be obtained.

XPS was used to examine the composition of the passivated cobalt NPs. The Co $2p_{1/2}$ and Co $2p_{3/2}$ peaks of cobalt NPs coated by TPP and OA were measured on the ESCA LAB5 x-ray photoelectron spectrometer with monochromated Mg x-rays at 10 kV. The structure of the NPs was examined using a Rigaku D/MAX 2400 x-ray diffractometer with Cu $K\alpha$ radiation ($\lambda = 1.5406 \text{ \AA}$). Samples for the XPS and XRD analysis were prepared by spreading several drops of cobalt dispersion on standard Si(111) wafers with a 150 nm thick SiO_2 layer and evaporating the solvent. A vacuum-transfer vessel was used to carry the sample from the drying box to the chamber without exposing the sample to the air. IR spectra of the samples were recorded using a Bruker EQUINOX55 at room temperature by dropping the colloid solution on a KBr tablet. Transmission electron microscopy (TEM) was used to determine particle size distribution and crystalline structure. LRTEM images were obtained on a JEOL-200CX operating at 120 kV and HRTEM images on a Philips CM200FEG operating at 200 kV. The samples were formed by drying heptane or by octane dispersion of cobalt NPs on amorphous-carbon-coated copper grids.

3. Results and discussion

XPS was used for particle surface element analysis. In XPS analysis, the penetration depth of the XPS beam used is between 3.0 and 5.0 nm while the chain length of the OA and the TPP is about 2.0 nm. So the depth probed from the surface of the cobalt NPs to the core of the cobalt NPs is between 1.0 and 3.0 nm, which ensures that the surface valence of the molecule-coated cobalt NPs can be obtained. Figure 1(a) is the XPS spectrum of the freshly prepared cobalt NPs. Characteristic peaks of cobalt, carbon and phosphorus are observed. Because the cobalt is the only nonvolatile product of the reaction, $[\text{Co}_2(\text{CO})_8] \rightarrow 2\text{Co} + 8\text{CO}$, and all the residual surfactant is removed by washing the precipitate

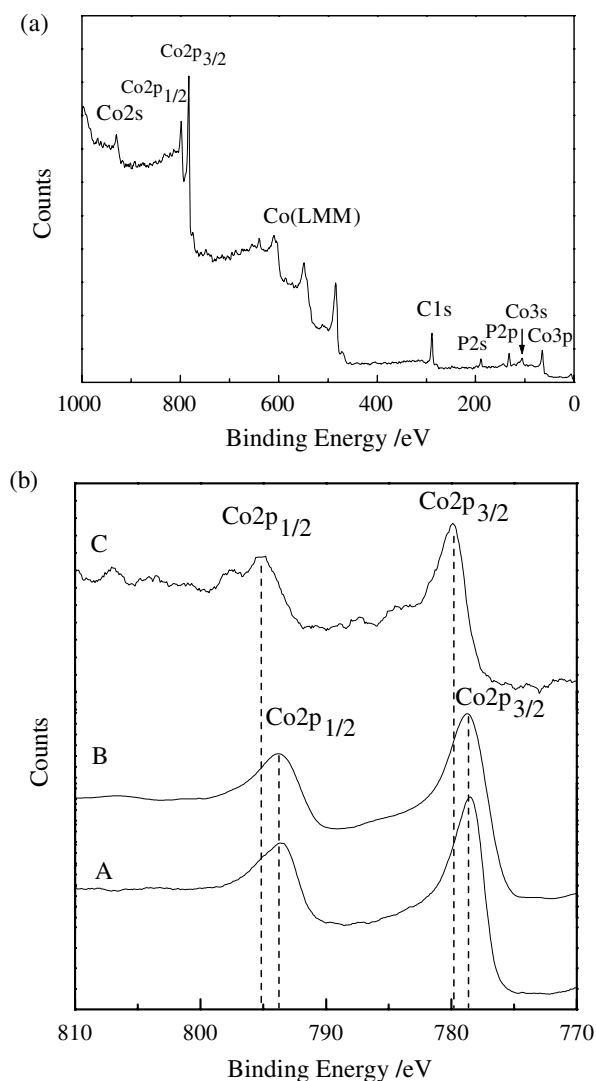


Figure 1. XPS spectra of (a) molecule-coated cobalt NPs, (b) Co 2p of cobalt NPs kept for one day (A), 90 days (B) and 120 days (C).

with ethanol several times, the characteristic peaks of carbon and phosphorus are introduced from the TPP and OA coated surface of cobalt NPs. According to the literature [18], OA and TPP should react or coordinate with the surface atoms of the Co NPs to prevent the oxidation or aggregation of Co NPs. Figure 1(b) is the XPS spectrum showing the Co $2p_{3/2}$ and Co $2p_{1/2}$ peaks of cobalt NPs from a dispersion kept under air for one day (curve A), 90 days (curve B) and 120 days (curve C). The Co $2p_{3/2}$ and Co $2p_{1/2}$ peaks of the cobalt NPs kept under air for one day are present at 778.5 and 793.6 eV, respectively. The difference between two peaks is 15.1 eV, which is consistent with the standard spectra of the element cobalt. XPS on cobalt NPs that have been kept in heptane under air for 90 days shows the same Co $2p_{3/2}$ and Co $2p_{1/2}$ peaks that are from the typical valence state of the Co^0 , indicating that the Co NPs in heptane are fairly stable against further oxidation. However, we do observe the valence change of cobalt from the Co NP sample that has been kept in heptane under air for 120 days. The binding energy of Co $2p_{3/2}$ and Co $2p_{1/2}$ now occurs at 779.9 and 795.4 eV, respectively, corresponding to the Co^{2+} oxidation state. Moreover, the peaks become broader

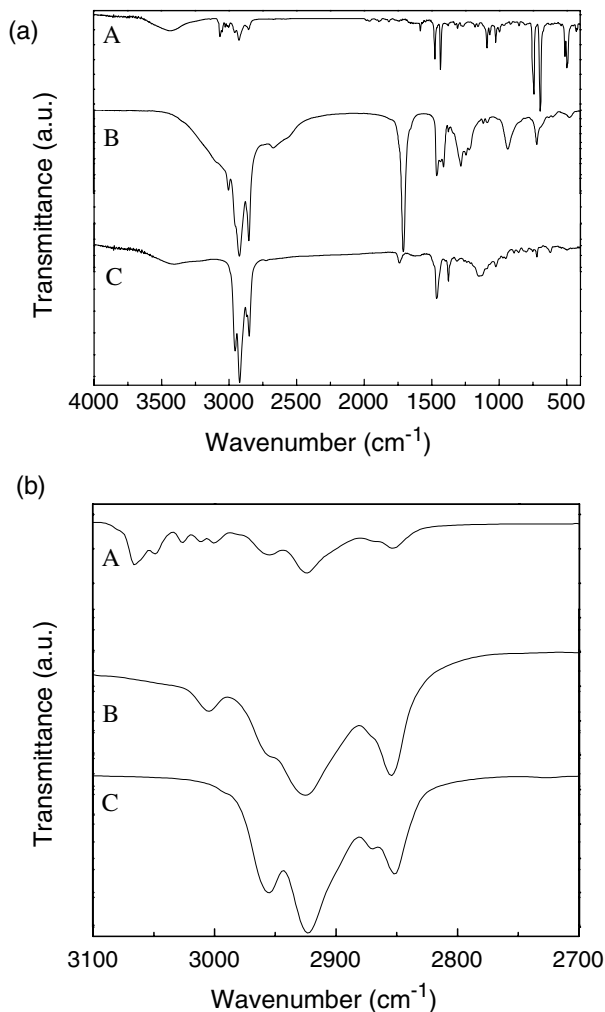


Figure 2. IR spectra of free TPP (curve A), free OA (curve B) and cobalt NPs coated by OA and TPP (curve C), where (b) is the high magnification spectrum of (a), with wavenumbers from 2700 to 3100 cm^{-1} .

and satellite peaks appear, which also indicates the change of the valence of the cobalt NPs.

The IR spectra of the free TPP, free OA and the cobalt NPs coated by OA and TPP are shown in figure 2. The IR absorptions provide information about the local molecular environment of the organic ligands on the nanoparticle surface. By comparing the IR spectra of the NPs and free surfactants in figure 2, we can see that the organic molecules have indeed become a part of the NPs. As shown in the figure, the peaks corresponding to C=O stretching at ~ 1710 and 1285 cm^{-1} , P- Φ stretching at 1711 cm^{-1} , the rocking and bending mode of the methylene group $\omega(\text{CH}_2)$ at 1270 cm^{-1} , the bending mode of the phenyl group $\gamma(=\text{CH})$ at 742 cm^{-1} and δ (benzene ring) = 697 cm^{-1} can be clearly seen. The only difference among these characteristic peaks is either the peak intensity or slight shift of the peak position. For example, the peak position of the longitudinal modes of the OA and TPP shifts to lower wavenumbers after TPP/OA are adsorbed on the surface of the cobalt NPs, appearing in the region of 2925 to 2923 cm^{-1} for $\nu_a(\text{CH}_2)$, 2854 – 2852 cm^{-1} for $\nu_s(\text{CH}_2)$ and 2958 – 2955 cm^{-1} for $\nu_s(\text{CH}_3, \text{ip})$. This is believed to be due to the organic molecules forming a relatively close-packed layer, thereby

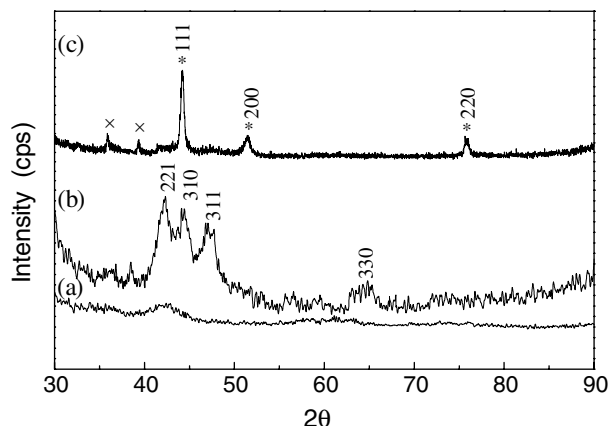


Figure 3. X-ray powder diffraction pattern of cobalt NPs passivated with $\text{C}_{18}\text{H}_{34}\text{O}_2/\text{C}_{18}\text{H}_{15}\text{P}$: (a) as-synthesized 3 nm particles, (b) as-synthesized particles of 7 nm and (c) after annealing at 500°C under Ar + H_2 (5%) for 3 h. Peaks corresponding to fcc cobalt are denoted by * and peaks corresponding to CoO are denoted by x.

constraining their own mobility on the surface of the NPs [19–21]. Thus, this steric constraint affects the transverse modes (rocking mode, wagging mode, etc) more than that on the longitudinal modes (stretching mode, etc). However, the peaks corresponding to the C=O stretching mode $\nu(\text{C}=\text{O})$ at 1710 and 1285 cm^{-1} disappear in curve C but the P- Φ stretching mode $\nu(\text{P}-\Phi)$ at 1434 cm^{-1} still appears in curve C though they both belong to a longitudinal mode. This is because the C=O band position is the closest to the surface of the cobalt NPs. From these results, a chemical bond can be formed between O and Co atoms while a coordinate bond forms between P and Co atoms around the nanoparticle on the surface. Thus, the C=O stretching mode disappears in the coated nanoparticle but the P- Φ stretching mode $\nu(\text{P}-\Phi) = 1434$ cm^{-1} is visible in curve C of figure 2.

X-ray diffraction of 3 nm TPP/OA passivated Co NPs as prepared showed a broad peak centred at $2\theta = 42.4^\circ$ (figure 3(a)). As the particle size increases, for example to 7 nm, the x-ray diffraction pattern (shown in figure 3(b)) can be identified as a crystalline structure which is similar to that of the β -manganese phase (a high-temperature phase of manganese), also called ε -cobalt. The ε -cobalt phase is metastable [22]. After annealing at 500°C under Ar (95%) + H_2 (5%) for 3 h, it can transform completely to the fcc phase (figures 3(c)). Subsequent cooling does not convert the fcc structure back to its original ε -cobalt structure. This is in good agreement with the ε -Co structure change observed elsewhere [23]. In figure 3(c), the small diffraction peaks of the cobalt oxide (CoO) are observed after the annealing. The average particle diameter can be estimated using Scherrer's formula [24]. The average size calculated from figures 3(b) and (c) is about 6.2 and 27.3 nm, respectively, indicating the agglomeration and the growth of the cobalt NPs during the annealing.

Slow evaporation of the heptane dispersion of cobalt NPs spread on a flat substrate allows well-organized superlattice structures to be formed. When the solution concentration is nearly 1%, the cobalt NPs are self-assembled into well-defined and extended 2D superlattices, as shown in figure 4. From the histogram of the size distribution and the TEM image, it can be concluded that the particles are uniform. The average diameter

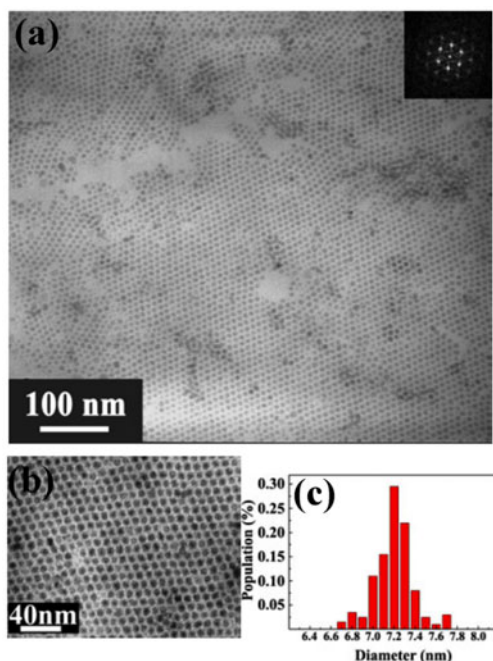


Figure 4. LRTEM image of a 2D superlattice of cobalt NPs shown at low (a) and higher (b) magnification. The 2D Fourier transform power spectrum of the image is inset in (a) and identifies a hexagonal close-packed (hcp) structure. (c) The histogram of the size distribution shows the average diameter of the NPs is 7.2 ± 0.5 nm. (This figure is in colour only in the electronic version)

of the NPs is 7.2 ± 0.5 nm and the average spacing between neighbouring particles is 1.9 nm. Controlled evaporation of octane dispersion of similar monodisperse cobalt NPs at 40°C leads to 3D superlattice structure. Figure 5 is the TEM image of the 3D superlattice of ~ 5 nm cobalt NPs. The ordered area in the 3D superlattices extends over $0.6 \mu\text{m} \times 0.6 \mu\text{m}$. Both 2D and 3D superlattices have a hexagonal stacking structure. The HRTEM image of the cobalt NPs, as shown figure 5(c), reveals complicated interference patterns, which are consistent with multiple crystal orientations contained within a single NP [25].

4. Conclusions

Cobalt NPs have been prepared using thermal decomposition of cobalt carbonyl in the presence of TPP and oleic acid. The as-synthesized cobalt particles show fairly good ϵ -Co crystallinity and are stable in hydrocarbon solvents against air oxidation. Controlled evaporation of the solvent from NP dispersions leads to 2D and 3D superlattices with hexagonal close-packing. Such monodisperse magnetic NPs and nanoparticle superlattices can be used as an ideal model for nanomagnetic studies.

Acknowledgments

The authors would like to thank S H Sun and M P Dotson for critical reading of the manuscript and Z Q Qiu for helpful discussions and suggestions. The project is partly supported by the National Nature Science Foundation of China (Grant no 90101025 and no 90206028) and National '973' and '863' of China.

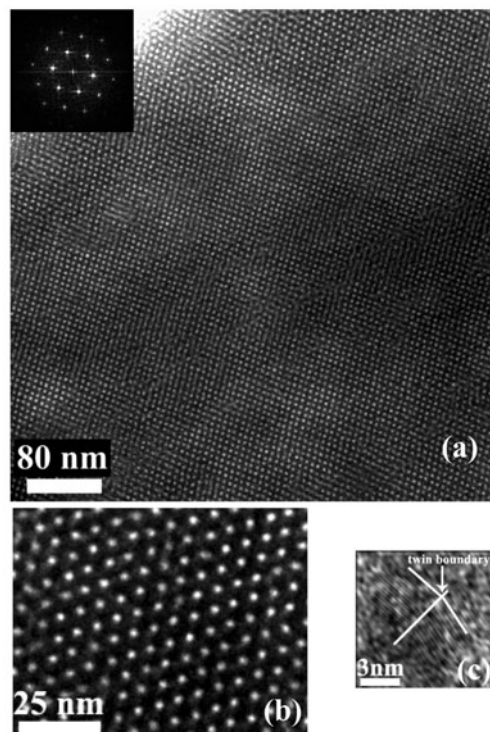


Figure 5. LRTEM image of a 3D superlattice of cobalt NPs shown at low (a) and higher (b) magnification. The Fourier transform power spectrum of the image is inset in (a). (c) HRTEM image of a single particle with a twin structure.

References

- [1] Zhang Z, Patel R C, Kothari R, Johnson C P, Friberg S E and Aikens P A 2000 *J. Phys. Chem. B* **104** 1176
- [2] Peng X, Wickham J and Alivisatos A P 1998 *J. Am. Chem. Soc.* **120** 5343
- [3] Valden M, Lai X and Goodman D W 1998 *Science* **281** 1647
- [4] Link S and El-Sayed M A 1999 *J. Phys. Chem. B* **103** 8410
- [5] He S T, Xie S S, Yao J N, Gao H J and Pang S J 2002 *Appl. Phys. Lett.* **81** 150
- [6] Gao H J, Sohlberg K, Xue Z Q, Chen H Y, Hou S M, Ma L P, Fang X W and Pennycook S J 2000 *Phys. Rev. Lett.* **84** 1780
- [7] Ma L P, Song Y L, Gao H J, Zhao W B, Chen H Y, Xue Z Q and Pang S J 2003 *Appl. Phys. Lett.* **69** 3752
- [8] Petit C, Talab A and Pileni M P 1999 *J. Phys. Chem. B* **103** 1805
- [9] Puentes V F, Krishan K M and Alivisatos A P 2001 *Science* **291** 2115
- [10] Murray C B, Norris D J and Bawendi M G 1993 *J. Am. Chem. Soc.* **115** 8706
- [11] Schmid G, Pfeil R, Boese R, Bandermann F, Meyer S, Calis G H M and van der Velden J W A 1981 *Chem. Ber.* **114** 3634
- [12] Feldheim D L, Grabar K C, Natan M J and Mallouk T E 1996 *J. Am. Chem. Soc.* **118** 7640
- [13] Clarke L, Wybourne M N, Brown L O, Hutchison J E, Yan M, Cai S X and Keana J F W 1998 *Semicond. Sci. Technol.* **13** A111
- [14] Walter W W, Scott M R, Marvin G W and James E H 2000 *J. Am. Chem. Soc.* **122** 12890
- [15] Andres R P, Bein T, Dorogi M, Feng S, Henderson J I, Kubiak C P, Mahoney W, Osifchin R G and Reifenberger R 1996 *Science* **272** 1323
- [16] Sun S 2002 *The 8th IUMRS Int. Conf. on Electronic Materials (Xi'an, China, June 2002)* p 382 (Book of abstracts)

- [16] Murray C B, Sun S, Gaschler W, Doyle H, Betley T A and Kagan C R 2001 *IBM J. Res. Dev.* **45** 47
- [17] Dinega D P and Bawendi M G 1999 *Angew. Chem., Int. Edn. Engl.* **38** 1788
- [18] Sun S and Murray C B 1999 *J. Appl. Phys.* **85** 4325
- [19] Ulan A 1991 *An Introduction to Ultrathin Organic Films: from Langmuir-Blodgett to Self-Assembly* (Boston: Academic)
- [20] Korgel B A, Fullam S, Connolly S and Fitzmaurics D 1998 *J. Phys. Chem. B* **102** 8379
- [21] He S, Yao J, Jiang P, Shi D, Zhang H, Xie S, Pang S and Gao H 2001 *Langmuir* **17** 1571
- Yang H T, Shen C M, Su Y K, Yang T Z, Wang Y G and Gao H J 2003 *Appl. Phys. Lett.* **82** 4729
- [22] Shoemaker C B, Shoemaker D P, Hopkins T E and Yidepit S 1978 *Acta Crystallogr. B* **34** 3573
- [23] Chen J M, Sorensen C M, Klabunde K J and Hadjipanayis G C 1995 *Phys. Rev. B* **51** 11527
- [24] Klug H P and Alexander L E 1962 *X-Ray Diffraction Procedures for Polycrystalline and Amorphous Materials* (New York: Wiley) p 491
- [25] Marks L D 1994 Experimental studies of small particle structures *Rep. Prog. Phys.* **57** 603